Fluid Structure Interaction Modelling of a Patient Specific Cerebral Aneurysm: Effect of Hypertension and Modulus of Elasticity

S. Ahmed[1], I. D. Šutalo[1], H. Kavnoudias[2] and A. Madan[2]

[1]Commonwealth Scientific and Industrial Research Organisation (CSIRO)
Materials Science and Engineering, Highett, Melbourne, Victoria, 3190, AUSTRALIA

[2]Radiology Department, The Alfred
Commercial Road, Melbourne, Victoria, 3004, AUSTRALIA

Abstract

This study investigates the computational coupled Fluid Structure Interaction (FSI) of a large wide neck cerebral aneurysm where the elastic aneurysm wall has non-linear deformation. A patient specific cerebral aneurysm geometry was obtained from CT medical scans. Computational Fluid Dynamics (CFD) was used to model the three-dimensional transient incompressible laminar non-Newtonian fluid flow through the aneurysm. For the structural analysis the aneurysm wall was assumed to be isotropic, incompressible and homogeneous. The effect of hypertension and modulus of elasticity were analysed in terms of fluid flow, wall shear stress, deformation and effective (Von-Mises) stress. The predictions showed the areas of the aneurysm that experience high stress and deformation. The aneurysm with hypertensive blood pressure (HBP) had higher stress and deformation compared to the normotensive blood pressure (NBP). The maximum deformation of the aneurysm wall increased with decrease in the wall modulus of elasticity. For a value of the Young's Modulus=25 MPa, the maximum deformation and effective stress increased rapidly due to the lateral movement of the aneurysm. Thus higher blood pressure as well as lower modulus of elasticity are important factors for the rapid aneurysm growth and rupture.

Introduction

Cerebral aneurysms are pathological dilatations of the vessel wall. The most serious consequence of cerebral aneurysms is their rupture and intracranial haemorrhage into the subarachnoid space with an associated high mortality rate [10]. In recent years various attempts have been made [1-2, 7] to investigate the hemodynamics and stress distribution of large cerebral aneurysms. Although extensive experimental and numerical investigations [9, 11-15] of flow velocity and flow visualization have been made on simplified cerebral aneurysms, the mechanisms of how cerebral aneurysms initiate, grow and rupture still remain uncertain. Several numerical investigations [3-5, 8] have been performed on patient specific cerebral aneurysms with rigid walls. There are fewer papers on simplified and patient specific cerebral aneurysms [16-19] dealing with FSI between the blood and the aneurysm wall. Valencia and Solis [19] described the flow dynamics and arterial wall interaction of a terminal aneurysm of simplified basilar artery and compared its wall shear stress, pressure, effective stress and wall deformation with those of a healthy basilar artery. They also investigated [19] the effect of wall modulus of elasticity in a range between 5 to 300 MPa and found that the effective stress distribution was independent of the modulus of elasticity. But the flow was assumed to be Newtonian. Torii et al. [16] studied the FSI of a patient specific cerebral aneurysm located in the left middle cerebral arterial bifurcation for high blood pressure but for a Newtonian fluid. They found that hypertension affects the growth

of an aneurysm and the damage in arterial tissues. They extended their investigation by comparing the effect of hypertension on two different shaped cerebral aneurysms and found that the wall deformation due to HBP was highly dependent on cerebral aneurysm geometry which stresses the importance of patient specific simulations [18]. To see the effect of wall modulus of elasticity Torii et al. [17] varied the Young's Modulus in simple pipe flow but then only used one value in simulation. The objective of this study is to investigate the effect of hypertension and modulus of elasticity on cerebral aneurysms where the bi-directional FSI modelling of a patient specific cerebral aneurysm includes a non-Newtonian fluid and an elastic wall that has non-linear deformation.

Description of the Cerebral Aneurysm

Cerebral aneurysms are frequently observed in the outer wall of curved vessels. They are found in the internal carotid artery, near the apex of bifurcated vessels including the anterior communicating artery, anterior cerebral artery and the middle cerebral artery. This paper presents the FSI investigation of a large, irregular and wide neck patient specific cerebral aneurysm located at the bifurcation of the left anterior cerebral artery (figure 1).
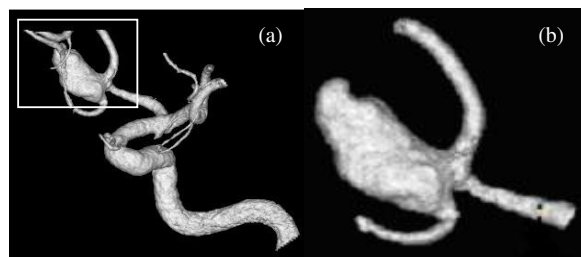

Figure 1. (a) Location of the cerebral aneurysm, and (b) Close - up of the cerebral aneurysm geometry used for modelling.

The neck width, maximum dome height, maximum dome width and artery diameter were 6.5 mm, 14 mm, 7.5 mm and 2.85 mm respectively. For the geometry reconstruction 38 CT slices with 0.6 mm intervals and 1 mm thickness were used. The surface of the arterial lumen was constructed first by using in-house software. Because the arterial wall cannot be seen with the CT scan, it was added by assuming a uniform wall thickness of 0.4 mm. The luminal wall was extended 0.2 mm in both inward and outward directions to create the arterial wall for the structural analysis. The volume mesh for the fluid flow analysis was generated by using commercial software ICEM CFD. ANSYS WORKBENCH was used to generate the mesh for the structural analysis. The meshes for the fluid flow and structural analysis are shown in figure 2.
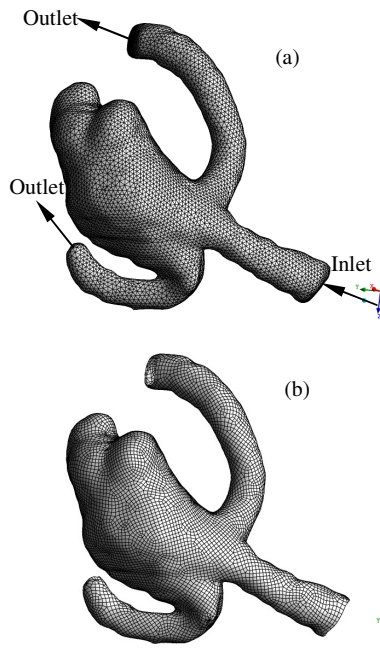
Figure 2. Aneurysm meshes for the (a) fluid flow analysis, and (b) structural analysis.

Numerical Modelling

For the fluid domain three-dimensional transient incompressible laminar flow fields were obtained by solving the continuity and Navier-Stokes equations. Numerical modelling was performed using a commercially available CFD package ANSYS-CFX-11 which has a coupled solver and uses an unstructured mesh based on the finite volume method. The inlet boundary condition was set by specifying a velocity pulse [6] at the inlet for a period of 0.8 s. The maximum and mean of the Reynolds numbers based on the parent vessel diameter were 500 and 98 respectively and the Womersley number, which characterizes the pulsatility of the flow, was 6.5. A pressure pulse [6] was applied at the two outlets. Simulations were performed for both NBP and HBP. The range of the NBP and HBP were 80-125 mmHg and 120-165 mmHg respectively. The boundary conditions are shown in figure 3.

The phase difference at the peak between the velocity (0.26 s) and the pressure (0.28 s) was taken into account in this investigation as recommended by Torii et al. [18]. The density of the blood was 1050 kg/m³. The non-Newtonian behaviour of blood was modelled by using Carreau's model. All the parameters for Carreau model were taken from Byun and Rhee [1]. Bi-directional FSI was used in this investigation where the blood exerts pressure to the artery wall, causing it to deform and, thus, alter the flow of the fluid.
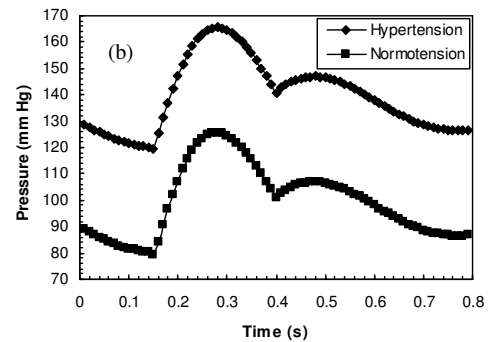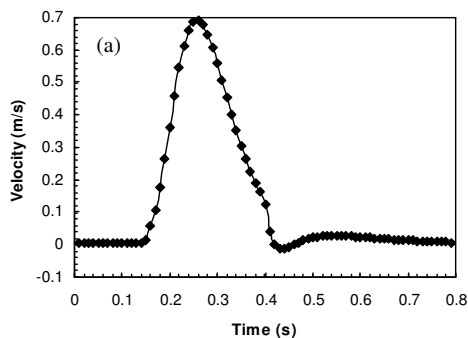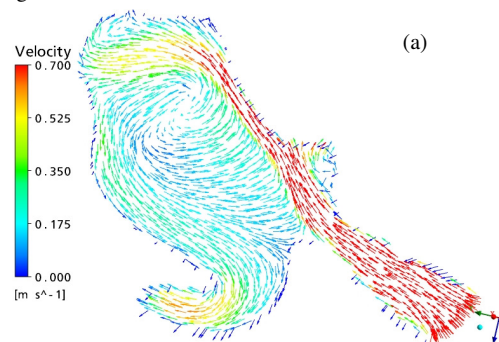

Figure 3. Boundary conditions for (a) inlet, and (b) outlet.

For the structural analysis commercially available software ANSYS-Mechanical was used. The governing equation for the structural domain was the momentum conservation equation. The artery wall was assumed to be elastic, isotropic, incompressible and homogeneous with a density of 1050 kg/m³ and a Poisson's ratio of 0.45. The non-linear deformation of the artery wall was considered in this investigation. Experimental results of elasticity studies in an aneurysm show that the Young's Modulus is as high as 300 MPa compared to 1 MPa for a normal artery [19]. A representative value of the Young's Modulus was taken as 50 MPa with a wall thickness of 0.40 mm to investigate the effect of hypertension. To study the effect of modulus of elasticity a range of Young's Modulus between 25 to100 MPa was chosen with the same wall thickness of 0.4 mm. The three ends of the artery were held fixed by specifying zero-displacement boundary conditions. In order to analyse the stress distribution in the aneurysm wall, the Von-Mises stress, used as a material fracture criteria in complicated geometries, was employed.

For the fluid flow the mesh consisted of tetrahedral elements. The solutions were mesh independent when the total number of elements for the fluid flow and structural analysis were 214,510 and 10,210 respectively. The time step used for this simulation was 0.005 s. The convergence criterion for the fluid flow and across the fluid structure interface were 10^{-4} and 10^{-3} respectively.

Effect of Hypertension
Flow Dynamics

The fluid flow pattern inside the aneurysm is complex and depends on the shape and size of the aneurysm geometry [3]. Figure 4 shows the comparison of the predicted velocity vector fields between the NBP and HBP cases at the peak systole (0.26 s) in the plane through the aneurysm shown in figure 5. For the NBP, the blood flow coming from the parent artery (inlet) impinged at the neck of the right branch and then divided into two parts. A major portion entered into the aneurysm sac with a high velocity (0.7 m/s), moved along the aneurysm wall, struck at the top of the dome, and finally exited from the aneurysm through the neck of the left branch.
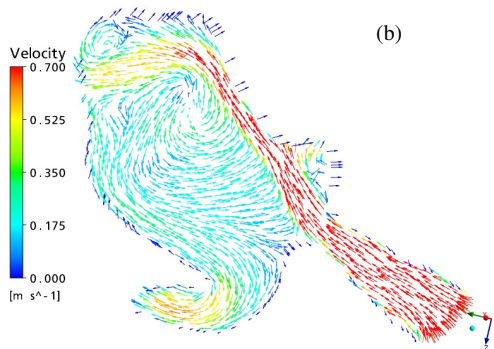
Figure 4. Comparison of the predicted velocity vector fields at peak systole (0.26 s) in the viewing plane for (a) NBP, and (b) HBP.

A large primary recirculation zone existed in the middle of the aneurysm sac together with a small secondary recirculation zone at the top of the dome. For the HBP the fluid flow pattern was similar to the NBP but the secondary recirculation zone became more prominent.
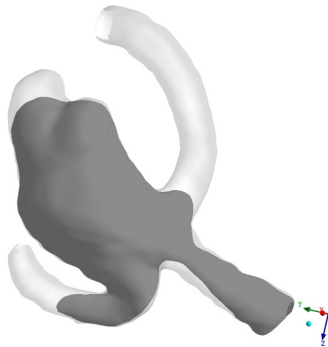

Figure 5. The plane at which comparisons of the predicted velocity vectors between the NBP and HBP is made.

Figure 6 shows the wall shear stress distribution at the peak systole (0.26 s) for the NBP and HBP. In both cases there were two local maxima (30 Pa) of the wall shear stress. One occurred on the aneurysm wall and the other on the wall of the right branch near the neck. The blood with a high velocity (0.7 m/s) impinged at the neck of the aneurysm at the right branch. As a result a high velocity gradient existed in this region which caused the high wall shear stress. There was a region in the parent artery where the wall shear stress was also high due to the irregular wall surface of the parent artery. While passing through the parent artery the high velocity flow struck the irregular surface which resulted in a sudden change in velocity in that region and consequently increased the wall shear stress. For this investigation HBP did not alter the wall shear stress distribution at the peak systole (0.26 s) which is consistent with Torii et al. [18] observation.
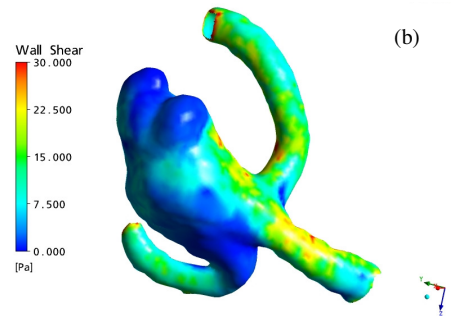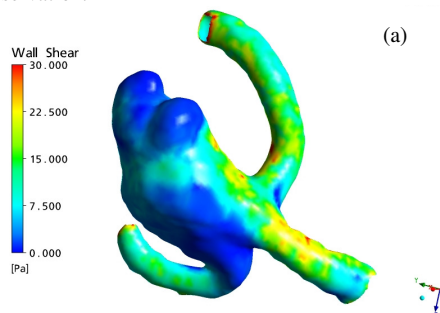

Figure 6. Comparison of the predicted wall shear stress at the peak systole (0.26 s) for (a) NBP, and (b) HBP.

Solid Dynamics

The deformation at the peak systole (0.26 s) due to pulsatile blood pressure is shown in figure 7. For both cases the maximum deformation occurred at the dome of the aneurysm wall. For the HBP case the maximum deformation (0.173 mm) was 37% higher than the NBP case (0.126 mm). The magnitude of the maximum deformation was approximately 4.4% and 6.0% of the parent artery diameter for the NBP and HBP respectively.
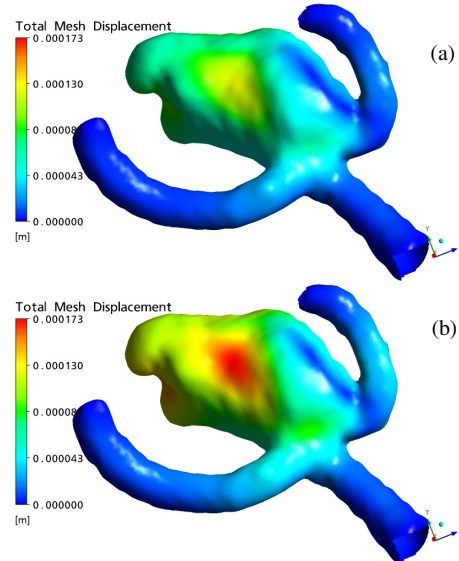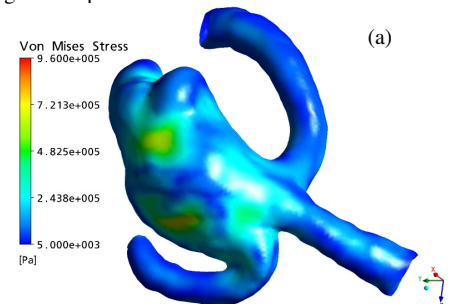

Figure 7. The predicted maximum deformation at the peak systole (0.26 s) for (a) NBP, and (b) HBP.

Figure 8 shows the effective (Von-Mises) stress distribution for the NBP and HBP at the peak systole. For the NBP, the effective stress was significantly higher (0.62 MPa) at the location of the maximum deformation, but the maximum stress (0.74 MPa) occurred on the other side of the dome (figure 8(a)). For the HBP case (figure 8(b)) the maximum effective stress (0.96 MPa) was 30% higher compared to the NBP case.
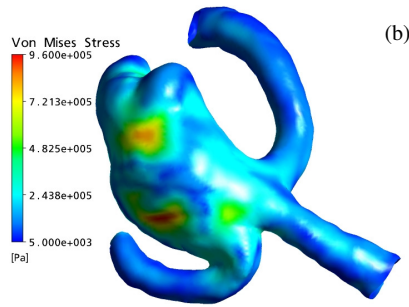
Figure 8. Distribution of the predicted effective (Von-Mises) stress at the peak systole (0.26 s) for (a) NBP, and (b) HBP.

Figures 9 and 10 show the comparison of the variation of the maximum deformation and maximum effective stress between the NBP and HBP for one cardiac cycle. The distribution of the maximum deformation closely resembled the pressure profile which indicates that primarily inflation of the aneurysm wall was responsible for the deformation. A similar trend was observed for the distribution of the maximum effective stress. From figure 10 it is evident that an increase in blood pressure increases the maximum effective stress and therefore increases the risk to rapid growth and rupture of the aneurysm.
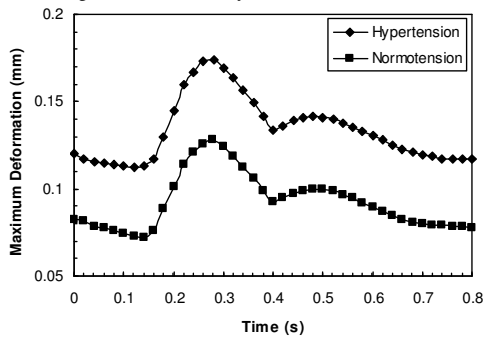

Figure 9. Variation of the predicted maximum deformation for one cardiac cycle.
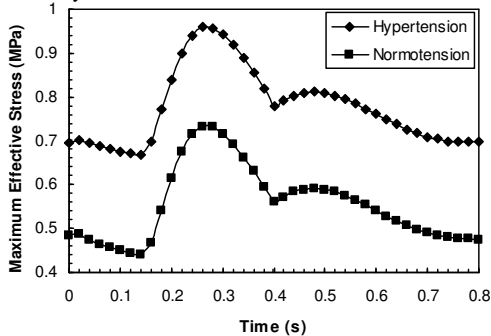

Figure 10. Variation of the predicted maximum effective (Von-Mises) stress for one cardiac cycle.

Effect of Modulus of Elasticity
The effect of modulus of elasticity was investigated for the NBP case with a 0.4 mm wall thickness by varying the Young's Modulus as 25, 30, 50 and 100 MPa. The results have been analysed in terms of flow dynamics and solid dynamics and have been explained below.

Flow Dynamics
The fluid flow pattern was same for the 30, 50 and 100 MPa cases, but there was a difference for the 25 MPa case due to deformation. Figure 11 shows the comparison of the predicted velocity vector fields between the 25 and 30 MPa cases at the

peak systole (0.26 s) in the viewing plane (figure 5). As there was no difference between the 30, 50 and 100 MPa cases, only the predicted velocity vector fields for 30 MPa case are shown.
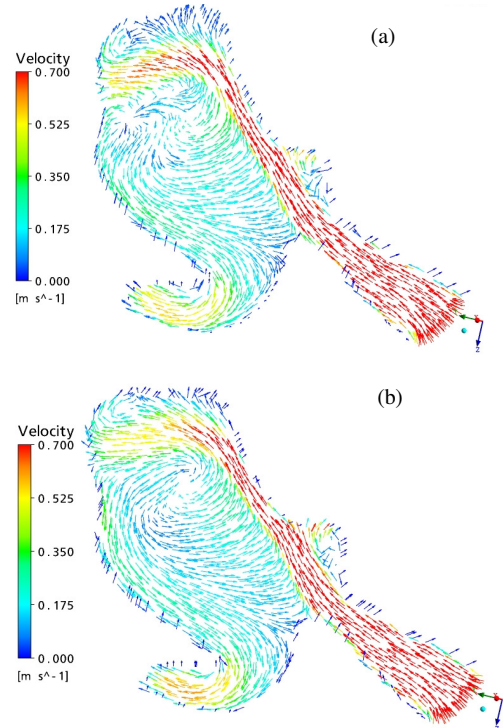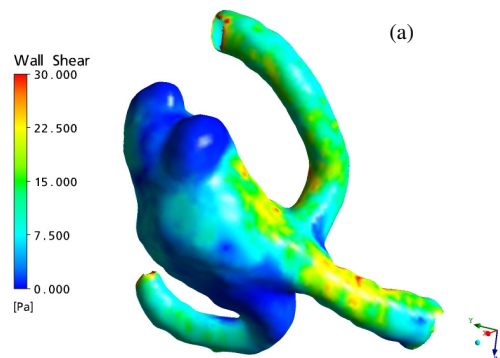

Figure 11. Comparison of the predicted velocity vector fields at peak systole (0.26 s) in the viewing plane for (a) 25 MPa, and (b) 30 MPa.

For the 25 MPa case, the formation of a counter rotating vortex pair was evident at the dome on the left side of the primary recirculation zone. The magnitude of the vortex pair was small in the viewing plane. A part of the flow from the counter rotating vortex moved towards the centre of the primary recirculation zone resulting in a more complex fluid flow pattern compared to the 30 MPa case.

Figure 12 shows the wall shear stress distribution at the peak systole (0.26 s) for the 25 and 30 MPa cases. The wall shear stress was independent of the modulus of elasticity and the results are consistent with the observation of Valencia and Solis [19] which cover the range of modulus of elasticity used in our study. The maximum wall shear stress (30 Pa) occurred on the aneurysm wall as well as on the wall of the right branch near the neck.
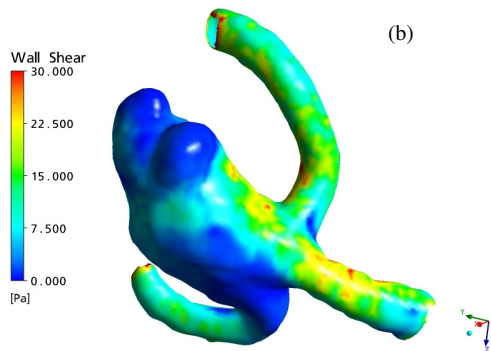
Figure 12. Comparison of the predicted wall shear stress at the peak systole (0.26 s) for (a) 25 MPa, and (b) 30 MPa.

Solid Dynamics

The distributions of the deformation for the different wall modulus of elasticity due to the pulsatile blood pressure are shown in figures 13 and 14. Figure 13 shows the comparison of the maximum deformation for the 50 and 100 MPa cases. For both of these cases the maximum deformation occurred at the peak systole (0.26 s) and at the dome of the aneurysm wall. For the 50 MPa case the maximum deformation (0.126 mm) was more than doubled than the 100 MPa case (0.058 mm). The magnitude of the maximum deformation was approximately 4.4% and 2.0% of the parent artery diameter for the 50 and 100 MPa cases respectively.
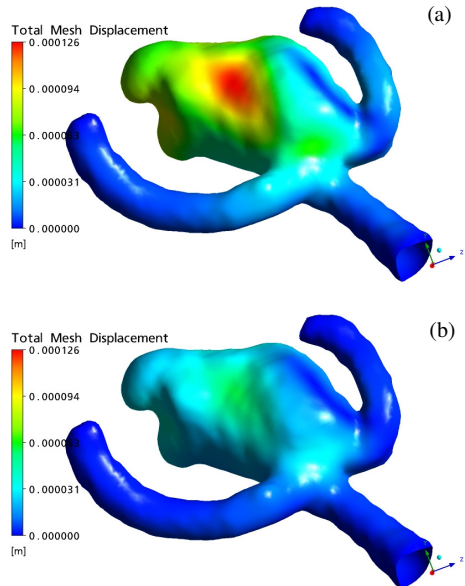

Figure 13. The predicted maximum deformation at the peak systole (0.26 s) for (a) 50 MPa, and (b) 100 MPa.

Figure 14 shows the comparison of the maximum deformation for the 25 and 30 MPa cases. For both cases the maximum deformation occurred at 0.30 s (for 25 MPa) and 0.29 s (for 30 MPa) respectively. The maximum deformation for the 25 and 30 MPa was 3.61 mm and 0.438 mm. The location of the maximum deformation changed from the dome to the top of the dome. The magnitude of the maximum deformation was approximately 127% and 15% of the parent artery diameter for the 25 MPa and 30 MPa cases respectively.

The mechanism of the maximum deformation was different for the 50 and 100 MPa cases compared to the 25 and 30 MPa cases.

For the 50 and 100 MPa cases only the inflation due to the pulsatile blood pressure was responsible for the deformation whereas for the 25 and 30 MPa cases deformation involves not only inflation but also the lateral movement of the top of the dome. This phenomenon can be explained more clearly from figure 15 where the comparison of the variation of the maximum deformation for one cardiac cycle has been plotted.
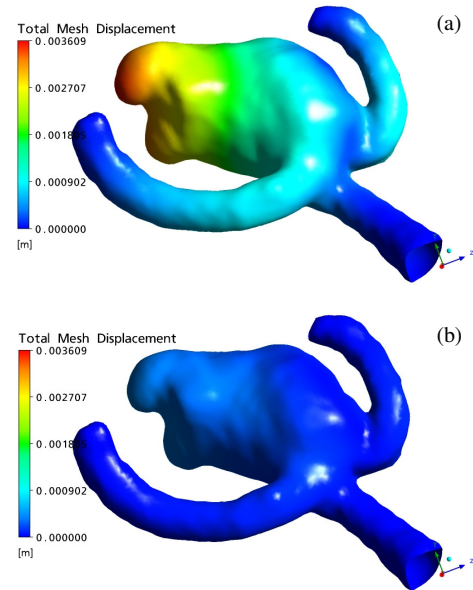

Figure 14. The predicted maximum deformation for various wall modulus of elasticity at (a) 0.30 s for 25 MPa, and (b) 0.29 s for 30 MPa.

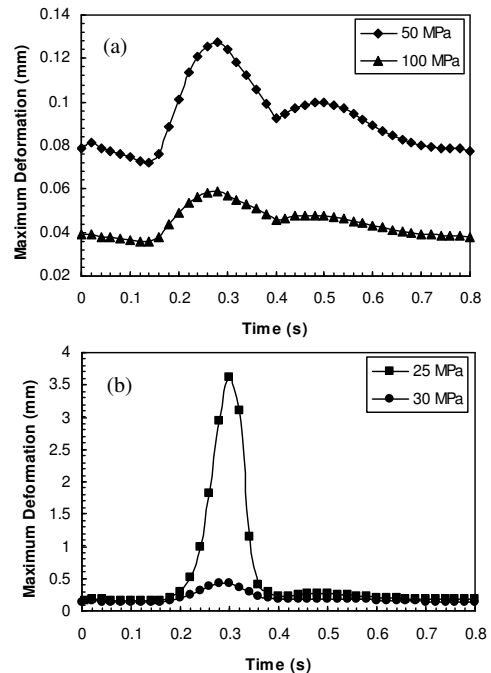Figure 15. Variation of the predicted maximum deformation for one cardiac cycle for various wall modulus of elasticity. (a) 50 and 100 MPa cases, and (b) 25 and 30 MPa cases.

Figure 15(a) shows the variation of the maximum deformation for the 50 and 100 MPa cases for one cardiac cycle. The distribution closely resembled the pressure profile indicates that the deformation is due to the inflation caused by the pulsatile

pressure. For the 25 and 50 MPa cases (figure 15(b)), the distribution was different in the range 0.2-0.38 s. The top of the dome started to move left at the mid acceleration phase (0.2 s), reached at the maximum after the peak systole (0.30 s) and came back to its original position at the end of the deceleration phase (0.38 s). The magnitude of the lateral movement was small compared to the magnitude of the inflation for 30 MPa case but was large for the 25 MPa case. This lateral movement occurred due to the shape and size of the aneurysm.

The effective (Von-Mises) stress distribution was independent of the modulus of elasticity for the 30, 50 and 100 MPa cases. The maximum effective stress (0.74 MPa) occurred at the peak systole (0.26 s) and at the dome of the aneurysm wall. As maximum effective stress was independent of the modulus of elasticity (for the range of 30 to 100 MPa) only the location of the maximum shear stress for the 30 MPa is shown in figure 16(a). The distribution for the 25 MPa case was different in the range 0.26-0.32 s and the maximum effective stress occurred after the peak systole (0.30 s). The value of the maximum effective stress was 1.35 MPa and located at the neck of the aneurysm wall as well as on the wall of the right branch near the neck as shown in figures 16(b) and 16(c). The location of the maximum effective stress differed for the 25 MPa case because of the large lateral movement of the top of the dome.
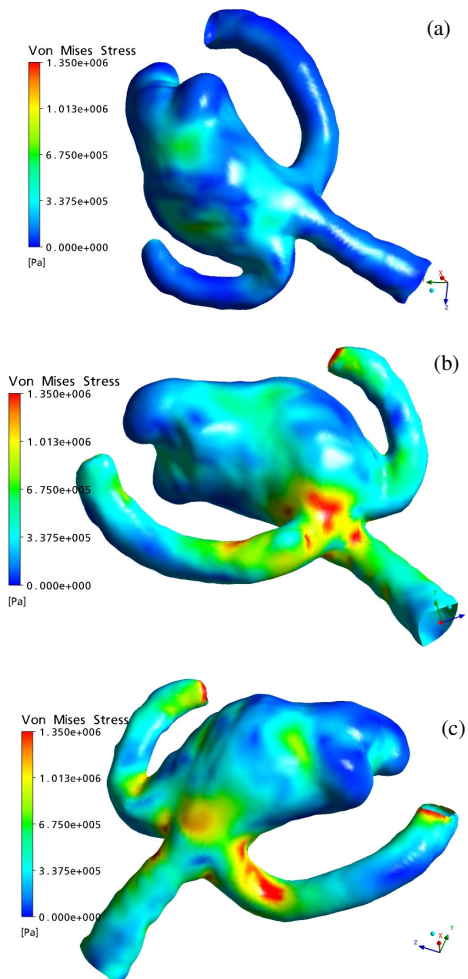

Figure 16. Distribution of the predicted effective (Von-Mises) stress with views showing the maximum stress for (a) 30 MPa case at the peak systole (0.26 s), and (b-c) 25 MPa case after the peak systole (0.30 s).

Figure 17 shows the variation of the maximum effective stress for the 25 and 30 MPa cases for one cardiac cycle. The maximum effective stress distribution for the 25 MPa case was the same as for the 30, 50 and 100 MPa cases except in the range 0.26-0.32 s where the maximum effective stress did not follow the pressure profile. It increased rapidly and changed the position of the maximum effective stress from the dome to the neck of the aneurysm wall at the peak systole (0.26 s) due to the large movement of the top of the dome, reached at the maximum at 0.30 s (figure 16 (b)), decreased rapidly and followed the pressure profile again from the mid deceleration phase (0.32 s). Valencia and Solis [19] investigated the effect of modulus of elasticity of a terminal aneurysm of basilar artery and found that the effective stress was independent of the Young's Modulus. As their study was on simplified symmetric geometry they did not find any difference in the effective stress distribution with the variation of wall modulus of elasticity. Our investigation revealed that modulus of elasticity is of the important factors for the rapid growth and rupture of the aneurysm and this paper highlighted the importance of having the correct modulus of elasticity when modelling the patient specific aneurysms.
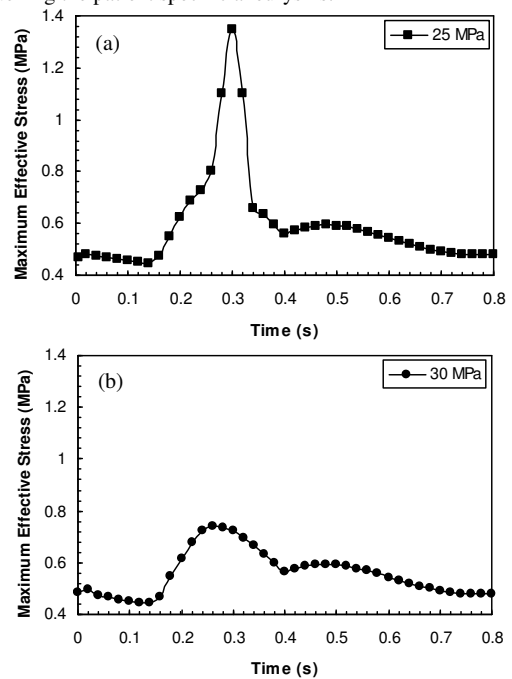

Figure 17. Variation of the predicted maximum effective (Von-Mises) stress for the (a) 25 MPa case, and (b) 30 MPa case for one cardiac cycle.

Conclusions

The effect of hypertension and modulus of elasticity on a patient specific large, irregular and wide neck cerebral aneurysm was investigated by using bi-directional FSI. Comparisons were made between the NBP and HBP cases and for a range of modulus of elasticity in terms of fluid flow, wall shear stress, deformation and effective stress. There was no significant difference at the peak systole (0.26 s) in the fluid flow and the wall shear stress between the NBP and HBP cases. But there was a clear difference when the deformation and the effective (Von-Mises) stress were compared. For an increase of 32% of the systolic pressure the maximum deformation for the HBP was 0.173 mm and was 37% higher compared to the maximum deformation (0.126 mm) of the NBP case. Similar results were found for the effective stress where the maximum value at the peak systole (0.26 s) was 30% higher for the HBP case. Comparisons for a range of wall modulus of elasticity (25-100 MPa) revealed that a

decreased in modulus of elasticity increase the maximum deformation of the aneurysm wall. The effective stress distribution was independent of the modulus of elasticity and followed the pressure profile for the 30, 50 and 100 MPa but was different for the 25 MPa in the range 0.26-0.32 s. The maximum effective stress increased rapidly in this range due to the lateral movement of the top of the aneurysm and therefore increased the risk to rapid growth and rupture of the aneurysm. This implies that hypertension and lower modulus of elasticity possibly affect the growth of aneurysm and lead to damage in the aneurysm wall. Thus, blood pressure and modulus of elasticity are important factors for the growth and rupture of cerebral aneurysms.

Acknowledgements

References

[1] Byun, H.S. & Rhee, K., CFD modeling of blood flow following coil embolization of aneurysms, *Med. Eng. Phys.*, **26**, 2004, 755-761.

[2] Byun, H.S. & Rhee, K., Intraaneurysmal flow changes affected by clip location and occlusion magnitude in a lateral aneurysm model, *Med. Eng. Phys.*, **25**, 2003, 581-589.

[3] Castro, M.A., Putman, C.M. & Cebral, J.R., Patient-Specific Computational Modeling of Cerebral Aneurysms with Multiple Avenues of Flow from 3D Rotational Angiography Images, *Acad. Radiol.*, **13/7**, 2006, 811-821.

[4] Castro, M.A., Putman, C.M. & Cebral, J. R., Computational Fluid Dynamics Modelling of Intracranial Aneurysms: Effect of Parent Artery Segmentation on Intra-Aneurysmal Hemodynamics, *Am J. Neuroradiol*, **27**, 2006, 1703-1709.

[5] Cebral, J.R., Castro, M.A., Soto, O., Lohner, R. & Alperin, N., Blood-flow models of the circle of Willis from magnetic resonance data, *J. Eng. Math.*, **47**, 2003, 369-386.

[6] Ganong, W.F., *Review of Medical Physiology*, 21st International Edition, McGraw Hill, 2001, 569.

[7] Gobin, Y.P., Counord, J.L., Flaud, P. & Duffaux, J., In vitro study of haemodynamics in a giant saccular aneurysm model: influence of flow dynamics in the parent vessel and effects of coil embolisation, *Neuroradiology*, **36**, 1994, 530-536.

[8] Hassan, T., Ezura, M., Timofeev, E. V., Tominaga, T., Saito, T., Takahashi, A., Takayama, K. and Yoshimoto, T., Computational Simulation of Therapeutic Parent Artery Occlusion to Treat Giant Vertebrobasilar Aneurysm, *Am J. Neuroradiol*, **25**, 2004, 63-68.

[9] Lieber, B.B.& Gounis, M.J., The physics of endoluminal stenting in the treatment of cerebrovascular aneurysms, *Neurol. Res.*, **24/1**, 2002, 33-42.

[10] Linn, F.H., Rinkel, G.J., Algra, A. & Van Gijn, J., Influence of subarachnoid haemorrhage: role of region, year and rate of computed tomography: a metaanalysis, *Stroke*, **27(4)**, 1996, 625-629.

[11] Liou, T-M., Chang, W-C. & Liao, C-C., Experimental Study of Steady and Pulsatile Flows in Cerebral Aneurysm Model of Various Sizes at Branching Site, *J. Biomech. Eng.*, **119**, 1997, 325-332.

[12] Liou, T-M. & Liou, S-N., Pulsatile Flows in a Lateral Aneurysm Anchored on a Stented and Curved Parent Vessel, *Exp. Mech.*, **44/3**, 2004, 253-260.

[13] Tateshima, S., Grinstead, J., Sinha, S., Nien, Y.L., Murayama, Y., Villablanca, J.P., Tanishita, K. & Vinuela, F., Intraaneurysmal flow visualization by using phase-contrast magnetic resonance imaging: feasibility study based on a geometrically realistic in vitro aneurysm model, *J. Neurosurg*, **100**, 2004, 1041-1048.

[14] Tateshima, S., Murayama, Y., Villablanca, J.P., Morino, T., Takahashi, H., Yamauchi, T., Tanishita, K. & Vinuela, F., Intraaneurysmal flow dynamics study featuring an acrylic aneurysm model manufactured using a computerized tomography angiogram as a mold, *J. Neurosurg*, **95**, 2001, 1020-1027.

[15] Tateshima, S., Vinuela, F., Villablanca, J.P., Murayama, Y., Morino, T., Nomura, K. & Tanishita, K., Three-dimensional blood flow analysis in a wide-necked internal carotid artery-ophthalmic artery aneurysm, *J. Neurosurg*, **99**, 2003, 526-533.

[16] Torii, R., Oshima, M., Kobayashi, T., Takagi, K. & Tezduyar, T.E., Fluid-structure interaction modeling of aneurysmal conditions with high and normal blood pressures, *Comput. Mech.*, **38**, 2006, 482-490.

[17] Torii, R., Oshima, M., Kobayashi, T., Takagi, K. & Tezduyar, T.E., Influence of wall elasticity in patient-specific hemodynamic simulations, *Comput. Fluids*, **36**, 2007, 160-168.

[18] Torii, R., Oshima, M., Kobayashi, T., Takagi, K. & Tezduyar, T.E., Numerical investigation of the effect of hypertensive blood pressure on cerebral aneurysm-Dependence of the effect on the aneurysm shape, *Int. J. Numer. Meth. Fluids*, **54**, 2007, 995-1009.

[19] Valencia, A. & Solis, F., Blood flow dynamics and arterial wall interaction in a saccular aneurysm model of the basilar artery, *Comput. Struct.*, **84**, 2006, 1326-1337.